Improving the ESA CCI Daily Soil Moisture Time Series with Physically Based Land Surface Model Datasets Using a Fourier Time-Filtering Method

EUNKYO SEO[a] AND PAUL A. DIRMEYER[a]

[a] *Center for Ocean-Land-Atmosphere Studies, George Mason University, Fairfax, Virginia*

(Manuscript received 22 June 2021, in final form 30 December 2021)

ABSTRACT: Models have historically been the source of global soil moisture (SM) analyses and estimates of land–atmosphere coupling, even though they are usually calibrated and validated only locally. Satellite-based analyses have grown in fidelity and duration, offering an independent observationally based alternative. However, satellite-retrieved SM time series include random and periodic errors that degrade estimates of land–atmosphere coupling, including correlations with other variables. This study proposes a mathematical approach to adjust daily time series of the European Space Agency (ESA) Climate Change Initiative (CCI) satellite SM product using information from physically based land surface model (LSM) datasets using a Fourier transform time-filtering method to match the temporal power spectra locally to the LSMs, which tend to agree well with in situ observations. When the original and timely adjusted SM products are evaluated against ground-based SM measurements over the conterminous United States, Europe, and Australia, results show the adjusted SM has significantly improved subseasonal variability. The skill of the adjusted SM is increased in temporal correlation by ~0.05 over all analysis domains without introducing spurious regional patterns, affirming the stochastic nature of noise in satellite estimates, and skill improvement is found for nearly all land cover classes, especially savannas and grassland. Autocorrelation-based soil moisture memory (SMM) and the derived random component of soil moisture error (SME) are used to investigate the improvement of SM features. The time filtering reduces the random noise from the satellite-based SM product that is not explainable by physically based SM dynamics; SME is usually diminished and the increased SMM is generally statistically significant.

KEYWORDS: Soil moisture; Satellite observations; Land surface model

1. Introduction

Land surface conditions play an important role in the development of extreme climate events, and many other processes related to the land–atmosphere interactions via the energy and water cycles (Dirmeyer et al. 2021; Seneviratne et al. 2010; Seo et al. 2020). In particular, soil moisture (SM) is a key component in hydrological and meteorological processes, which is designated an essential climate variable by the World Meteorological Organization (WMO), having a persistence or memory that can contribute to forecast skill at time scales up to at least 1–2 months (i.e., subseasonal; Dirmeyer et al. 2018; Dirmeyer et al. 2016; Seo et al. 2019). Daily soil moisture data are used to estimate many key land–atmosphere coupling metrics (Santanello et al. 2018). Realistic SM estimates are necessary to understand the comprehensive water, energy, and carbon cycles at the land surface. One efficacious way to produce a global observationally based SM product is from remote sensing retrievals derived from active and passive microwave satellite sensors.

Despite the increasing availability of SM data from remote sensing, it is difficult to obtain a self-consistent long-term soil moisture dataset because the lifespans of satellites are relatively short. To produce such a long-term SM product, Dorigo et al. (2017) combined data from various single-sensor active and passive microwave SM instruments into a combined global satellite-based observational SM dataset with multidecadal time coverage, produced as part of the European Space Agency's (ESA) Climate Change Initiative (CCI) program. There are three harmonized ESA CCI SM products: a merged ACTIVE, a merged PASSIVE, and a COMBINED active + passive microwave product. Comparison of the three different harmonized products shows the correlation coefficient of daily SM time series is highest against in situ measurements in the COMBINED product, while the skill of the PASSIVE product is slightly better than that of the ACTIVE after version v03.3 (Gruber et al. 2019). Furthermore, when the skill of a merged product like the ESA CCI SM is compared with the skill of the single-sensor products, the merged product generally shows comparable or superior performance (Dorigo et al. 2015).

However, all satellite SM products have systematic and random errors (Dorigo et al. 2010; Gruber et al. 2020; Su et al. 2016). Systematic error is attributed to biases in retrieval algorithms, inaccurate auxiliary data, and surface properties, which may be corrected by removing relative differences between the considered datasets (Gruber et al. 2016). Systematic representativeness errors that arise from different spatial resolutions and from spatial and temporal disagreement can be explained by resampling approach and be corrected by statistical rescaling methods (Gruber et al. 2020; Lei et al. 2018). Random errors may be caused by radiometric instrument performance, stray background microwave contributions within the sensors' field of view, view angle variations, spatial resampling, and imperfect parameterizations used in retrieval

Supplemental information related to this paper is available at the Journals Online website: https://doi.org/10.1175/JHM-D-21-0120.s1.

Corresponding author: Eunkyo Seo, eseo8@gmu.edu

DOI: 10.1175/JHM-D-21-0120.1

algorithms. Random errors especially undermine the ability to use these products to properly evaluate SM dynamics such as the rapid wetting by precipitation, and particularly the gradual desiccation of soil by infiltration and evapotranspiration. These errors, in particular, can greatly hamper the estimation of land–atmosphere coupling and feedbacks (Dirmeyer et al. 2016) and hinder the use of satellite soil moisture to evaluate and improve coupled land–atmosphere models.

Removal of erroneous signals not due to physically based SM dynamics can improve the utility of satellite SM data for water cycle process studies, model calibration, and validation. Triple collocation has been shown to be an effective method to identify errors and produce improved soil moisture analyses by combining independent datasets (Draper et al. 2013; Gruber et al. 2017). Su et al. (2013) proposed a physically based Wiener filter [referred to as Wiener water balance (WiWB)] to reduce stochastic random and systematic periodic errors in passive and active microwave satellite SM time series, in which the denoising method based on spectral analysis quantifies the difference between a theoretical power spectrum based on a water balance model and an empirical power spectrum from the satellite SM dataset. Su and Ryu (2015) first proposed an analysis framework, which combines multiresolution analysis and triple collocation, to demonstrate scale-dependent biases and enable multiscale bias correction of nonlinear denoising via wavelet shrinkage technique. Massari et al. (2017) formally introduced the Wiener wavelet (WiW) filter, which combines the robustness of the entropy-based wavelet denoising method (EBWDM) and the real-time applicability of a causal filter, demonstrated in an extensive intercomparison against other denoising methods, namely the WiWB and the moving averaging filter (MVAVG). The results addressed the main advantages of WiW and WiWB filters compared to MVAVG: their higher robustness, low sensitivity to oversmoothing, less subjectivity in the temporal window size and lack of necessity for additional ancillary data for calibration.

However, these noise reduction methods have some limitations. Despite the empirical water balance model underlying the WiW and WiWB filters, the underlying assumptions pertaining to noise and the linear approximation for the loss term without the impact of the change of the radiation flux in terms of the energy balance do not ensure a physically realistic time series. In other words, these filters, to be optimized, require local stationarity of the signal and a slowly moving mean, whereas actual SM is generally nonstationary and influenced by other conditions. The MVAVG method assumes that nearly all the high-frequency components below a certain frequency threshold are noise, which means that the method can distort the character of the time series. In the production of a long-term SM product, the effect of the low-frequency variability change in the precipitation and other land surface variables should be physically reflected in the SM variability. Otherwise, a physical imbalance between the ground-related variables and SM may appear, and limitations in studying long-term SM may result. Meanwhile, triple collocation derives its effectiveness by statistically combining observational and model soil moisture estimates, but for model validation and development a purely observational and model-independent dataset is preferable. It is a challenge to characterize and account for non-physically-related noise in satellite soil moisture estimates without unduly affecting the physically driven component of the time series.

In our effort to produce an improved global soil moisture dataset to estimate land–atmosphere coupling metrics, we have examined approaches to filter noise from long microwave satellite SM time series leveraging information from the physically based constraints inherent in land surface model (LSM) simulations. A Fourier transform method that focuses on the difference in noise characteristics between observations and models has been chosen based on the following objectives. The first objective is to quantify improvements that can be realized in ESA CCI SM time series through the adjustment of variance amplitude in harmonics based on information from several different LSMs with independent formulations. A key distinguishing feature of the filtering method is a physics-constrained approach to resolve nonstationary SM dynamics using information from physically based numerical models across the entire time series domain. The model SM and the improvement relative to the original ESA CCI SM are assessed against independent in situ soil moisture measurements. The second objective is to improve two key SM features in the original and time-filtered ESA CCI SM products: (i) soil moisture memory (SMM) and (ii) estimated soil moisture error (SME). We assess the benefit of the physically based SM time filtering in the context of global SM features as well as point validation against in situ observations.

The paper is organized as follows. Section 2 introduces the datasets used in this study. Section 3 describes the SM time filter methodology, and our validation approach to measure SM improvement. Section 4 presents and discusses the results of this study. Finally, section 5 summarizes the results and their implications for future applications.

2. Data

a. ESA CCI SM

The ESA CCI SM v06.1 combines four scatterometer-based active and 10 radiometer-based passive microwave sensors from various orbital platforms over a period of four decades. The C-band (5.3 GHz) Active Microwave Instrument Wind Scatterometer (AMI-WS *ERS-1/2* SCAT, 1991–2006; AMI-WS *ERS-2*, 1997–2007) and the C-band (5.3 GHz) Advanced Scatterometer (ASCAT) *MetOp-A* (2007–19) and *MetOp-B* (2012–19) have active sensors. Five passive sensors measure in the C-band (6.6 GHz) Scanning Multichannel Microwave Radiometer (SMMR, 1979–87), the K-band (19.3 GHz) Special Sensor Microwave Imager (SSM/I, 1987–2013), the X-band (10.7 GHz) Tropical Rainfall Measuring Mission (TRMM) Microwave Imager (TMI, 1998–2015), the X-band (10.7 GHz) *FengYun-3B* Microwave Radiation Imager (*FY-3B*/MWRI, 2011–19), and the X-band (10.7 GHz) Global Precipitation Measurement (GPM, 2014–20). Another three platforms measuring passively within the X band and C band are the Advanced Microwave Scanning Radiometer for Earth Observing System (AMSR-E, 2002–11), WindSat (2007–12), and the Advanced Microwave Scanning Radiometer 2 (AMSR2, 2012–19). The other two passive sensors measure in

the L band (1.4 GHz) from the Soil Moisture and Ocean Salinity (SMOS, 2010–19) and the Soil Moisture Active and Passive mission (SMAP, 2015–19). The ESA CCI SM algorithm harmonizes and merges these multiple active and passive satellite SM retrievals to generate a consistently intercalibrated and quality-controlled SM product with a larger spatial and temporal coverage than any single-sensor SM products. The combined dataset merging all active and passive products covers 41 years (1979–2020) at 0.25° spatial resolution, has a temporal resolution of ~1 day and a sensed soil thickness of ~5 cm, but it does contain gaps at places and times when and where no measurements were available. Comparisons to ESA CCI SM v05.2 are included in the online supplemental material.

b. Offline LSM datasets

The Global Land Data Assimilation System (GLDAS) was developed with the purpose of providing optimal land surface states and fluxes for global applications (Rodell et al. 2004). The system drives offline global gridded LSMs with observed near surface atmospheric variables to calculate the time evolution of land states and fluxes. The GLDAS-2.1 product provides near-real-time global land surface variables from 2000 to present; this study specifically uses the Noah LSM product. The observed atmospheric surface conditions come from the 3-hourly Global Data Assimilation System (GDAS) released by the National Centers for Environmental Prediction (NCEP) and hourly surface radiative fluxes and daily precipitation from the Air Force Weather Agency (AFWA) Radiation and the Global Precipitation Climatology Project (GPCP; Huffman et al. 2001). The GLDAS-2.1 SM product using the Noah LSM is reported for four soil layers (0–10-, 10–40-, 40–100-, and 100–200-cm depth) with a horizontal spatial resolution of 0.25° and a 3-hourly temporal resolution.

The European Centre for Medium-Range Weather Forecasts (ECMWF) Reanalysis version 5 Land (ERA5-Land) is an offline simulation of the Tiled ECMWF Scheme for Surface Exchanges over Land incorporating land surface hydrology (H-TESSEL) LSM forced by the ERA5 climate reanalysis that is the latest (fifth generation) global climate reanalysis dataset released by ECMWF, but the ERA5 near surface atmospheric temperature, humidity and pressure used to run ERA5-Land are corrected to account for the altitude difference between the lower resolution of ERA5 and ERA5-Land. ERA5-Land is the uncoupled open-loop companion to the atmospheric module of the ECMWF's Integrated Forecasting System (IFS) and is run without land data assimilation, compared to ERA5. The reason we adopt the ERA5-Land rather than ERA5 is the resolution of its SM product (ERA5 is at a lower resolution than ESA CCI) and the better representation of SM dynamics that avoids the violation of water balance closure due to analysis increments in the data assimilation scheme. ERA5-Land has four soil layers (0–7-, 7–28-, 28–100-, and 100–289-cm depth) with a horizontal spatial resolution of ~0.1° and an hourly temporal resolution.

The Modern-Era Retrospective Analysis for Research and Applications, version 2 (MERRA-2; Gelaro et al. 2017) reanalysis dataset also provides a separate land surface product simulated by the Catchment model (Koster et al. 2000) which is the land component of the Goddard Earth Observing System version 5 (GEOS5). The Catchment LSM is driven by its assimilated atmospheric variables in "replay" mode and the bias of the simulated precipitation is further corrected with gauge- and satellite-based precipitation observations. MERRA-2 provides surface (0–5 cm) and root-zone (0–100 cm) soil moisture with a spatial resolution of 0.625° × 0.5° and 1-hourly temporal interval. There is no direct soil moisture assimilation, so the surface water balance is preserved.

Data from all offline models are averaged to daily means for use in this study and the three LSMs are arithmetically averaged to produce a multimodel ensemble (MME) mean with the representative behavior of soil moisture variability simulated by different land surface physics. Averaging multiple LSMs results in a superior soil moisture analysis when verified against in situ observations (Guo et al. 2007), and in the absence of calibration data a simple mean performs consistently well (Guo and Dirmeyer 2006). When comparing soil moisture skill of each modeled and MME product against in situ observations over the United States (described in the next subsection), the skill of MME ($R = 0.73$) is higher than that of the other ($R = 0.62$, 0.68, and 0.69 in GLDAS-2.1, MERRA2, and ERA5_land, respectively) over the conterminous United States (CONUS). Although averaging ignores different soil moisture characteristics from different models, this study employs the MME with the philosophy that the superior input data to the models results in the best performance in the application (Guo et al. 2006).

c. In situ SM measurements

For validation over the continental domain, this study uses in situ soil moisture measurements from the International Soil Moisture Network (ISMN; Dorigo et al. 2011). We focus on three regions that provide relatively high spatial densities of observations. Over the CONUS, the Atmospheric Radiation Measurement (ARM), FLUXNET–AMERIFLUX, Cosmic-Ray Soil Moisture Observing System (COSMOS; Zreda et al. 2012), Plate Boundary Observatory (PBO H2O; Larson et al. 2008), Soil Climate Analysis Network (SCAN; Schaefer et al. 2007), Snowpack Telemetry (SNOTEL), U.S. Climate Reference Network (USCRN; Diamond et al. 2013; Bell et al. 2013), U.S. Department of Agriculture Agricultural Research Service (USDA-ARS; Jackson et al. 2010) network datasets are used for the validation. FR_Aqui (Al-Yaari et al. 2018), Danish Hydrological Observatory and Exploratorium (HOBE; Bircher et al. 2012; Jensen and Refsgaard 2018), ORACLE, REMEDHUS (González-Zamora et al. 2019), Soil Moisture Observing System–Meteorological Automatic Network Integrated Application (SMOSMANIA; Albergel et al. 2008; Calvet et al. 2007), and Terrestrial Environmental Observatories (TERENO; Zacharias et al. 2011) network datasets are used for validation over the Europe. The OZNET (Smith et al. 2012) network is used for validation over Australia. For validation, this study uses only the hourly measurements down to 5-cm depth with "good" quality flagged and simultaneously measured. After screening of the hourly data, we

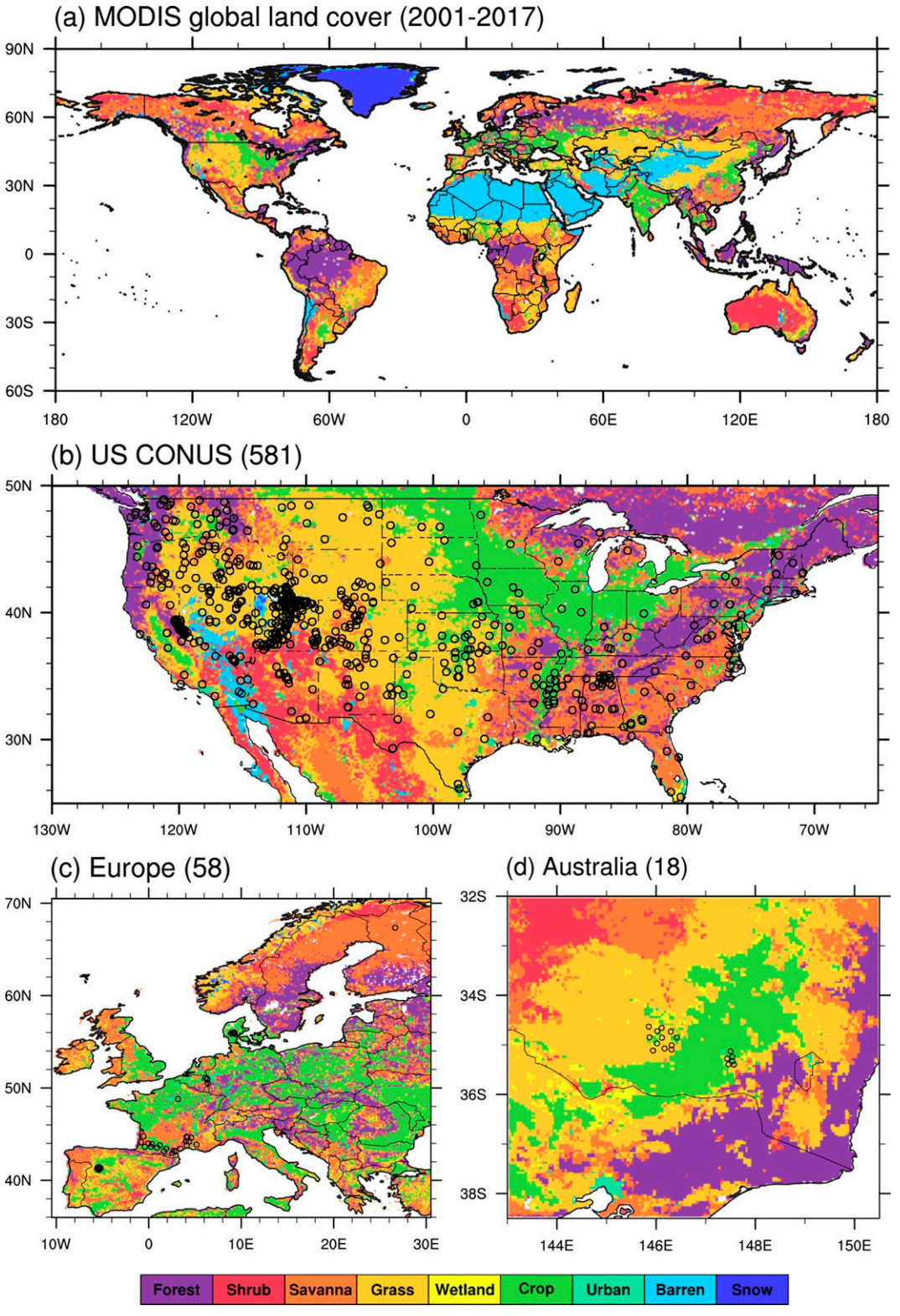

FIG. 1. Spatial distribution of climatological MODIS land cover classes for 2001–17 over (a) global, (b) CONUS, (c) Europe, and (d) southern east Australia. The open circles represent the location of ISMN monitoring sites used for validation (the number in parentheses in each subtitle indicates the number of in situ observations within the domain).

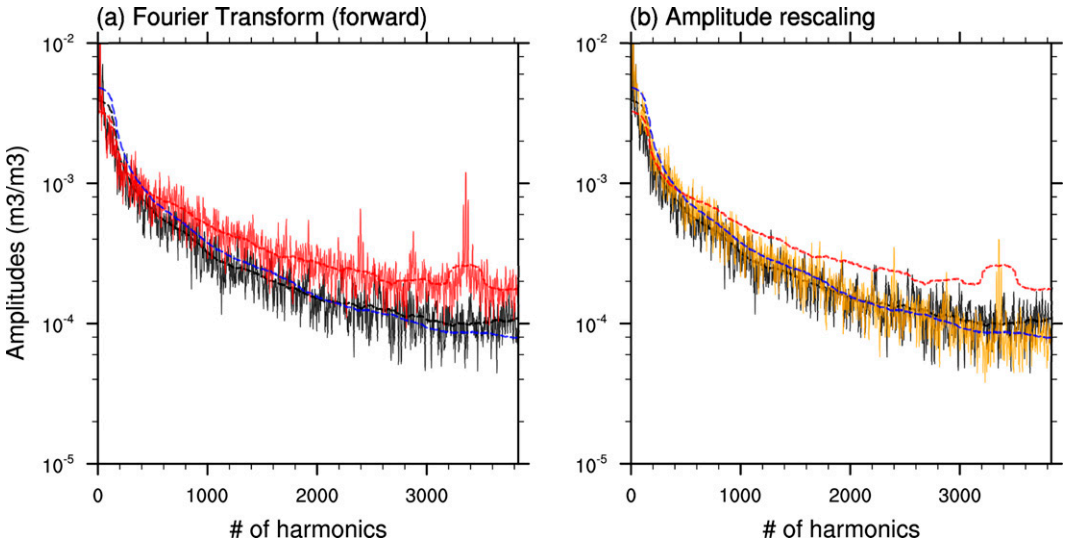

FIG. 2. (a) Example harmonic analysis of surface SM from in situ measurement (black), LSM MME (blue), and CCI (red) at Grouse Creek station (42.78°N, 113.82°W) in Utah. (b) Adjusted CCI SM harmonics (gold) after rescaling in each harmonic. Solid and dashed lines are 7- and 300-harmonic running averaged amplitudes, respectively.

calculate daily mean soil moisture and only sites with more than 30% of the entire validation date range are used.

Validation results are broken down by land cover type (Fig. 1). Land cover categories are from the MODIS Collection 5 product (Friedl et al. 2010) for 2001–17, which provides data at 500-m spatial resolution using 17 International Geosphere–Biosphere Programme (IGBP) classifications (Loveland and Belward 1997): 1) evergreen needleleaf forests, 2) evergreen broadleaf forests, 3) deciduous broadleaf forests, 4) deciduous needleleaf forests, 5) mixed forests, 6) closed shrubland, 7) open shrublands, 8) woody savannas, 9) savannas, 10) grasslands, 11) permanent wetlands, 12) croplands, 13) urban and built-up lands, 14) cropland/natural vegetation mosaics, 15) permanent snow and ice, 16) barren, and 17) water. For categorization by land cover, we group the IGBP classes into forest (1–5), shrubland (6–7), savannas (8–9), grassland (10), wetland (11), cropland (12 and 14), urban (13), barren (16), and snow (15) classes. For each of the gridded soil moisture products, validation is performed on the grid cell containing the in situ observation site.

3. Methodology

As mentioned before, satellite retrievals will contain some degree of random error due to the vagaries of instrument-based measurement. In situ observations of soil moisture may contain systematic errors (biases) depending on instrument calibration, but are generally considered to be accurate enough for purposes of process understanding and model validation. In-ground SM probes have considerably smaller random error than other instrument types; remote sensing is especially prone to high degrees of noise, even if the sensor is only meters from the soil surface (Dirmeyer et al. 2016). This noise necessarily inflates estimates of variance, degrades correlation calculations including autocorrelation (used to estimate SMM and SME) and affects estimates of metrics of land–atmosphere coupling.

In contrast, all the offline LSM datasets described above can be considered as being ultimately precise (i.e., they free from random measurement errors, generating nothing but "signal" from an information perspective) but are not necessarily accurate because of model parameter errors, parameterization shortcomings or missing processes. Errors or biases may exist in the atmospheric forcing terms contributing to the surface water budget (Reichle et al. 2004), thus affecting the rate of change of surface soil moisture. However, LSM time series will add no random "noise" as the values of simulated soil moisture at each model time step will be completely constrained by model physics and precise within computational limits. That is, an LSM adds no noise as it is deterministic—the same time series of input always produces the same time series of output.

Gridding of precipitation observations and other meteorological data to Earth system model resolutions acts as a partial filter on measurement noise. The reddening of the forcing spectrum as an LSM integrates through time to predict soil moisture acts as an additional noise filter on the observationally based atmospheric forcings, namely, precipitation. Thus, variance in model time series is strongly controlled by temporal variations in the gridded observationally based meteorological forcing modulated by LSM parameters (soil texture, land cover type, etc.) and parameterizations, providing a reasonable target for adjusting the spectrum of satellite soil moisture estimates. Because of evidence that variations in surface soil depth have little consequence for the temporal variability of SM within ~10-cm depth (Dirmeyer et al. 2016), comparison of model surface soil moisture with microwave-based estimates from satellite is reasonable.

In this study, we combine soil moisture datasets at the daily time scale for the 21-yr period 2000–20 to provide estimates of noise-free power spectra of surface soil moisture. The global gridded soil moisture products from LSMs are regridded to 0.25° spatial resolution corresponding to the ESA CCI SM. They are utilized in the correction of the ESA CCI daily SM time series

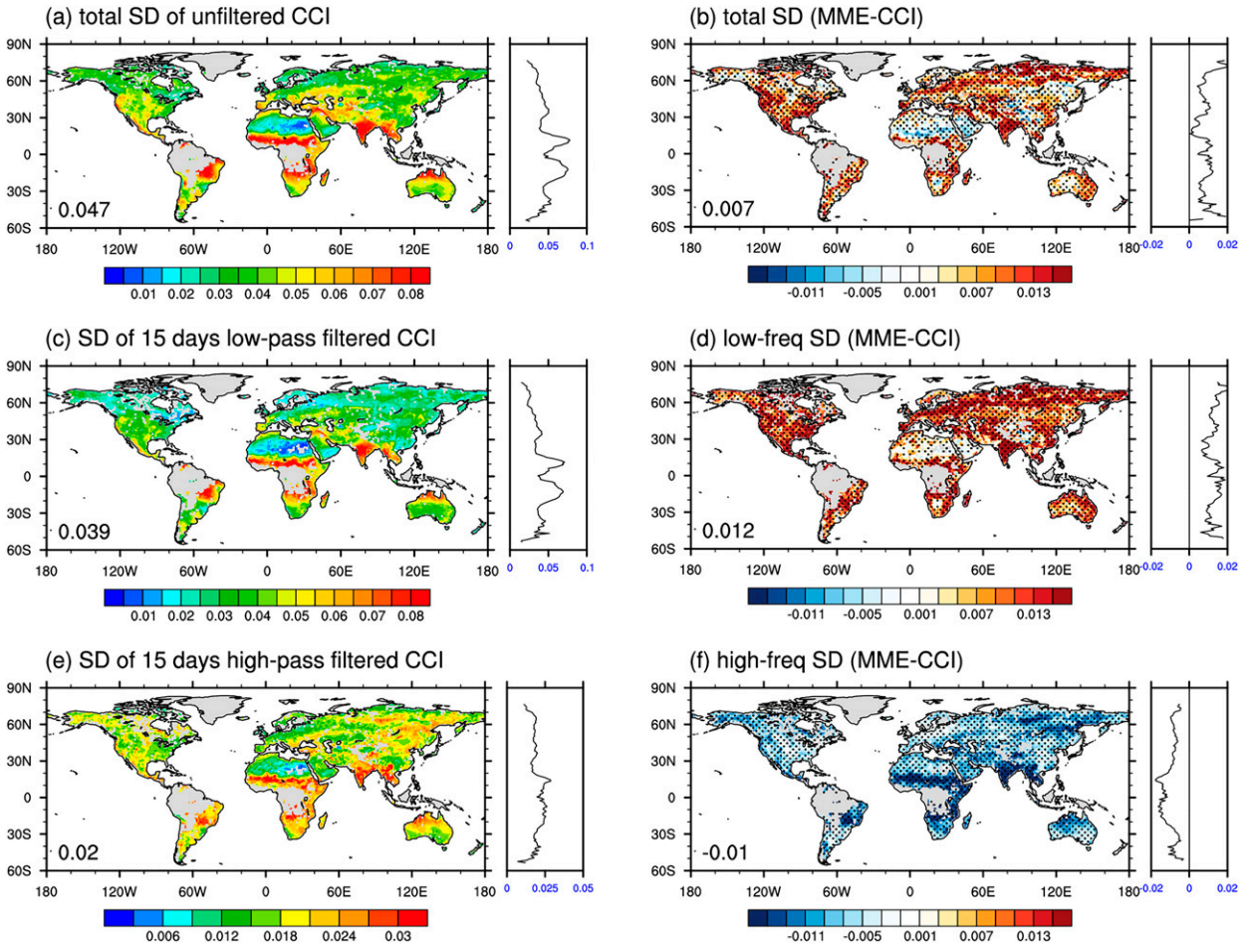

FIG. 3. Standard deviation of (a) unfiltered, (c) >15-day low-pass filtered, and (e) <15-day high-pass filtered CCI. SD difference of (b) total, (d) low, and (f) high frequency between LSM MME and CCI surface SM. The zonal mean is shown on the right of each panel. Globally mean values are indicated in the lower-left corner of each map. Dotted area represents statistical significance of the SD difference at a 95% confidence level from a Monte Carlo method.

in an attempt to minimize the imprint of random observational errors without degrading accuracy. In this section, we describe the Fourier transform-based method used to adjust the ESA CCI SM time series and the validation strategy applied to evaluate the performance of the timely corrected ESA CCI SM.

a. Gap filling

Since the satellite-based SM dataset does not provide spatially and temporally complete data for the daily and global scales, we fill missing values using information from the MME of the three LSM simulations. If we know SM values at two times (t_1 and t_2) bounded by the ends of the missing data period, we can estimate a regression line for t in the temporal domain as

$$\mathrm{Reg}(t) = \frac{[\mathrm{SM}(t_2) - \mathrm{SM}(t_1)]}{t_2 - t_1}\, t + \mathrm{SM}(t_1), \tag{1}$$

where SM is the SM value for a specified time. Based on the regression function from MME and CCI SM datasets, we gap-fill the CCI dataset for missing time ranges as

$$\mathrm{SM}_{\mathrm{CCI}}(t) = \mathrm{SM}_{\mathrm{MME}}(t) - \mathrm{Reg}_{\mathrm{MME}}(t) + \mathrm{Reg}_{\mathrm{CCI}}(t). \tag{2}$$

However, there is a possibility that $\mathrm{SM}_{\mathrm{CCI}}(t)$ attains a negative value at one or more time steps in this procedure. In that case, we modify Eq. (2) by multiplying an additional factor that rescales $\mathrm{SM}_{\mathrm{MME}}(t)$ variability:

$$\mathrm{fac} = \frac{\mathrm{Max}\,(\mathrm{SM}_{\mathrm{MME}}) - \mathrm{Min}\,(\mathrm{SM}_{\mathrm{MME}})}{\mathrm{Max}\,(\mathrm{SM}_{\mathrm{MME}})}, \tag{3}$$

where $\mathrm{Max}(\mathrm{SM}_{\mathrm{MME}})$ and $\mathrm{Min}(\mathrm{SM}_{\mathrm{MME}})$ are the maximum and minimum values of $\mathrm{SM}_{\mathrm{MME}}$ for the missing time range. Using MME for gap filling provides consistency with the following step.

b. Fourier-based time series correction

Based on the gap-filled CCI SM dataset, we perform a Fourier analysis on the harmonic spectra. A forward Fourier transform is applied separately to the modeled LSM SM and gap-filled CCI SM time series at each grid point across the entire time period.

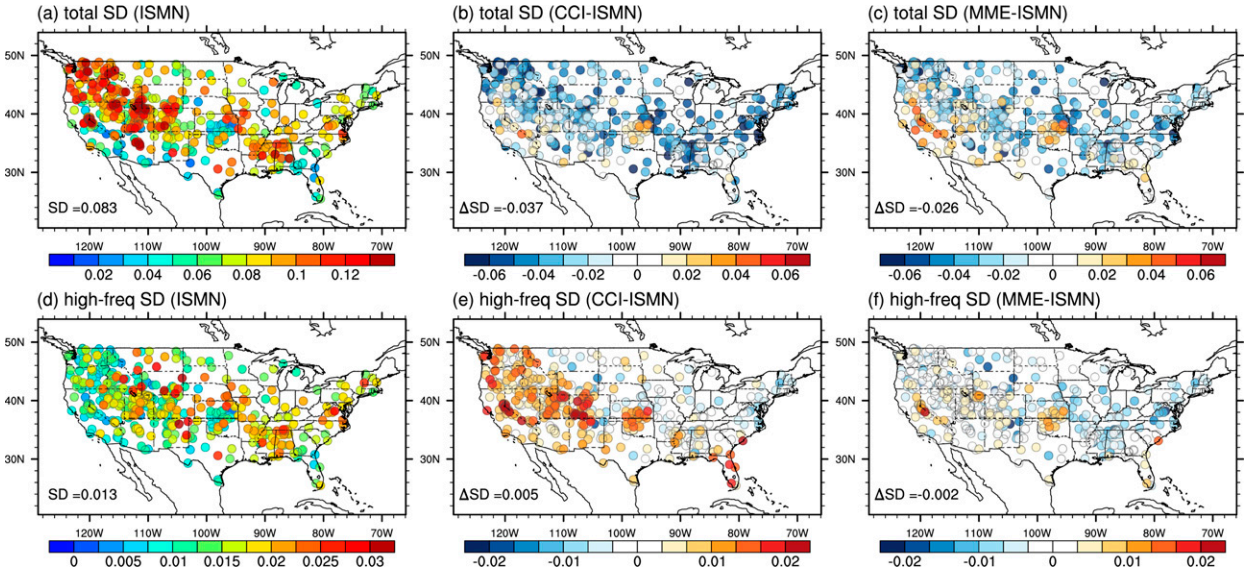

FIG. 4. (a) Total and (d) high-frequency surface SM SD of ISMN in situ observations. The bias of total and high-frequency surface SM SD in (b),(e) CCI and (c),(f) LSM MME against the observations, respectively. Domain averaged SD or its bias (ΔSD) are indicated in the lower-left corner on each map.

The same transform is performed on the in situ time series where available. We obtain the amplitude of each harmonic and a centered 300-harmonic running mean for each time series. Figure 2a shows an example at one location, but as shown in the next section, the agreement between MME and in situ time series is generally much better than for either with the remote sensing product. While maintaining the unique information in the CCI SM, we adjust the amplitude of all harmonics from the satellite-based SM to agree with that of the MME, based on the centered 300-harmonic running means. This size of averaging window in harmonic space is chosen because the 300 lowest-frequency harmonics are found to account for an average of ~90% of the variance of modeled surface soil moisture; results are found to be insensitive to moderate variations in this choice (not shown).

This correction considers both the relative difference between MME and CCI 300-harmonic running means and the anomaly of the amplitude of each CCI harmonic relative to the running mean:

$$\mathrm{Amp}_{\mathrm{CCI}_{\mathrm{adj}}}(h) = \frac{\mathrm{Amp}^{300}_{\mathrm{MME}}(h)}{\mathrm{Amp}^{300}_{\mathrm{CCI}}(h)}\,\mathrm{Amp}_{\mathrm{CCI}}(h), \tag{4}$$

where $\mathrm{Amp}_{\mathrm{CCI}}$ is the harmonic amplitude from the forward Fourier transform of the gap-filled CCI SM. The terms $\mathrm{Amp}^{300}_{\mathrm{MME}}$ and $\mathrm{Amp}^{300}_{\mathrm{CCI}}$ are the 300-harmonic running averaged amplitude for the MME and the CCI SM, respectively. The impact is shown in Fig. 2b in which the rescaled amplitude for the number of harmonics (h) is shown at a representative location: Grouse Creek station in Utah, United States. After the Fourier-based amplitude correction, the SM variability across the range of harmonics represents the observed power spectrum well. An updated daily ESA CCI SM time series is reconstructed via the backward Fourier transform of the adjusted spectrum. During the backward Fourier transform, the zero-frequency component ($h = 0$) from the gap-filled CCI mean is retained unaltered to preserve the CCI time mean. This approach can result in negative soil moisture values in a few grid cells. At such locations, standard normal deviate scaling (SNDS; Koster et al. 2004; Seo et al. 2019) is employed that reduces SM variability enough to prevent negative SM while preserving the mean value. Hereafter, we refer to the adjusted ESA CCI SM based on the LSM simulations as $\mathrm{CCI}_{\mathrm{adj}}$.

c. Validation strategy

For a fair comparison of the reconstructed $\mathrm{CCI}_{\mathrm{adj}}$ and LSM SM products to the original CCI SM, we mask out days in which the original CCI SM is missing. Additionally, frozen land surface conditions are masked out whenever the modeled surface temperature is less than 274 K. To validate the statistical significance in the comparison between CCI and $\mathrm{CCI}_{\mathrm{adj}}$ products, we apply a Student's t test. In addition, the statistical significance of the difference of standard deviations between CCI and MME SM products is tested using a Monte Carlo approach. The null-test probability distribution of the standard deviation of CCI is estimated by random resampling, where the standard deviation is calculated 1000 times with a randomly sampled time series for half of the time samples. Statistical significance is determined at the 95% level with a two-tailed test relative to the random distribution.

Each is validated against the in situ measurements described in section 2c. This study primarily evaluates the skill of the SM products in terms of local temporal variations using the Pearson correlation coefficient (R) applied to daily values of the surface SM.

Furthermore, we evaluate the surface SMM and the estimated SME. As Vinnikov and Yeserkepova (1991) proposed, the behavior of the daily SM time series fits a first-order

Markov process: its autocorrelation (r) at lag day (τ) can be defined by

$$r(\tau) = \exp(-f\tau), \tag{5}$$

where f is the SM decay frequency. We estimate the SMM as the lag at which the autocorrelation of SM drops to $1/e$. Robock et al. (1995) demonstrated a linear fitting of $\ln(r)$ as a function of τ using observational data, where SMM is calculated as the value of τ where linear extrapolation between $\ln[r(\tau = 1)]$ and $\ln[r(\tau = 2)]$ intersects $\ln(r) = -1$ (i.e., $r = 1/e$). The displacement of the linear extrapolation at $\tau = 0$ is the SME (a), a quantification of the degradation of autocorrelation estimates due to random errors. By shifting the linear best fit of $\ln(r)$ by a so as to intersect 0 at $\tau = 0$ (i.e., an autocorrelation of 1 at lag 0), the corrected estimate of SMM is the time lag in which the shifted line is intersected to $\ln(r) = -1$ (Dirmeyer et al. 2016). This is referred to as the "corrected" SMM, which is adopted in this study to measure the SM persistence for in situ measurements, CCI, and CCI_{adj} SM.

4. Results

a. Evaluation of surface SM variability

First, we examine the standard deviation (SD) of the daily CCI and MME SM products during the entire period in terms of low and high frequency as well as total variability. The SD of MME SM is calculated as the square root of multimodel mean SM variance. Figure 3 shows the spatial distribution of the surface SM SD in CCI and its difference map to MME SM products, along with their zonal means. The total SD of CCI shows the highest variability in tropical regions (Fig. 3a), but MME has statistically significantly higher variability over mid- to high-latitude regions (Fig. 3b). The spatial patterns are similar for the low-frequency (15 days low-pass filtered) SM (Fig. 3c) whereas the globally averaged amplitude of SD for MME is 30% higher than that of the CCI (0.039 $m^3\ m^{-3}$), where the higher variability of MME is more prominent (Fig. 3d) compared with the difference pattern of the total SD (cf. Fig. 3b). On the other hand, the high-frequency (15-day high-pass filtered) variability in CCI (0.02 $m^3\ m^{-3}$) is twice that of the MME (0.01 $m^3\ m^{-3}$) with nearly global statistical significance, in which there is a particularly large discrepancy over the tropics (Figs. 3e,f).

Such a comparison does not tell which product is better, so we have compared the SM SD of CCI and MME to in situ measurements over CONUS (Fig. 4). The total surface SM SD of the observations is high in the western United States north of ~37° latitude and over the southeastern United States (Fig. 4a) and the high-frequency variability is quite high in the central United States (Fig. 4d). The bias of the total surface SM SD from the MME versus observations (−0.024 $m^3\ m^{-3}$) is clearly less than that of the CCI (−0.037 $m^3\ m^{-3}$), while there is still an underestimation in the modeled SM variability (Figs. 4b,c). The low-frequency variability is similar to the total variability (not shown). The high-frequency surface SM SD from CCI (0.005 $m^3\ m^{-3}$) shows a strong positive bias of 38%, especially over the western United States, but such a large bias is not evident in

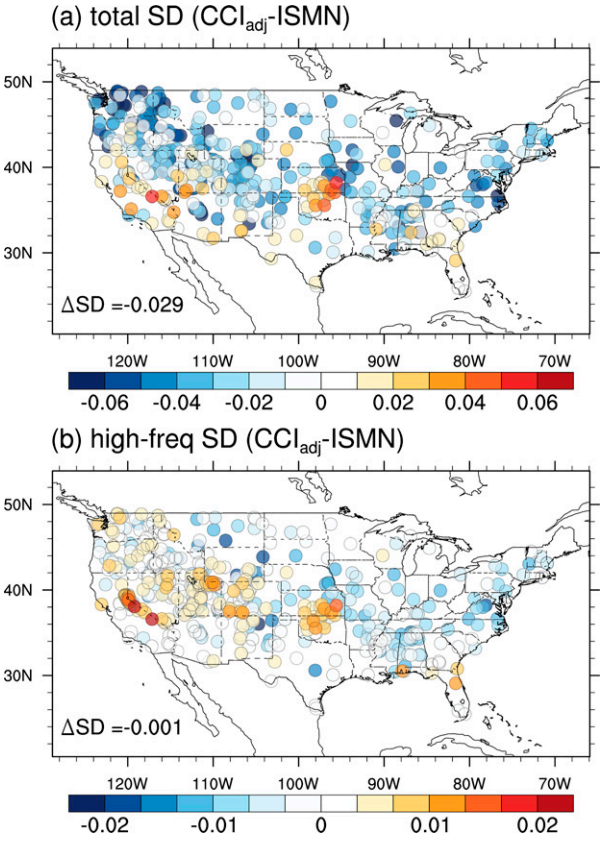

FIG. 5. The bias of (a) total and (b) high-frequency surface SM SD in CCI_{adj} against the observations. Domain averaged bias (ΔSD) is indicated in the lower-left corner on each map.

the MME (−0.002 $m^3\ m^{-3}$). Moreover, the spatial pattern of the high-frequency surface SM SD from MME ($R = 0.21$) is significantly better than that from CCI ($R = -0.08$) (Fig. 3e).

Vinnikov et al. (1996) noted that ground-based SM observations contain random error, and the total SM variance can be separated into the unbiased and error terms. When we isolate the unbiased SM variance from the random error in surface observations, there is no statistically significant difference; the random error in total and high-frequency in situ SM SD is only about 0.001 $m^3\ m^{-3}$ on average.

After applying the Fourier transform to the original CCI dataset on daily time intervals, we find the corrected surface SM demonstrates improved variability in total (Fig. 5a) and particularly high-frequency time domains (Fig. 5b). For total SM variability, the CCI represented an underestimation of 45%, but total CCI_{adj} variability underestimation (−0.029 $m^3\ m^{-3}$) drops below 35%. There is large overestimation in high-frequency variability in CCI (cf. Fig. 4e), but that large bias is diminished for CCI_{adj} (−0.001 $m^3\ m^{-3}$). Thus, the Fourier-based variability correction results in a more realistic daily SM power spectrum.

To address the noise reduction in the CCI daily SM time series through the time filtering, Fig. 6 presents an example of the daily time series of surface SM from in situ observations, CCI, CCI_{adj}, and ERA5_land as well as daily observed and

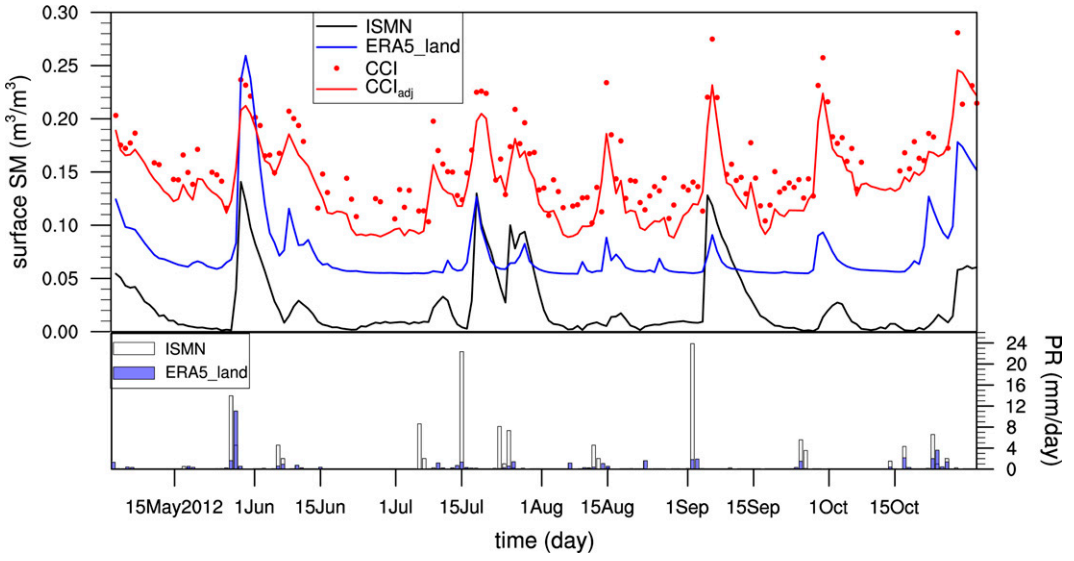

FIG. 6. Time series of surface SM of in situ observations (black line), CCI (red dots), CCI_{adj} (red line), and ERA5_land (blue line) at Grouse Creek station (42.78°N, 113.82°W) for May–October 2012. The bottom graph represents the daily time series of observed precipitation (open bars) and ERA5_land gridded precipitation forcing (blue bars).

ERA5_land precipitation at Grouse Creek station in Utah during May–October 2012. The observed SM time series is closely related to the precipitation via the surface water budget equation and ERA5_land shows such a SM response despite its underestimation of precipitation. CCI_{adj} clearly captures the smoothness of the observed daily SM evolution much better than the original version of CCI. As the surface water budget equation is in terms of land surface fluxes and the SM tendency, not the actual water storage, the systematic difference between the SM climatologies is addressed here, although such a difference could be a problem in other applications (e.g., agriculture, water resources, drought monitoring).

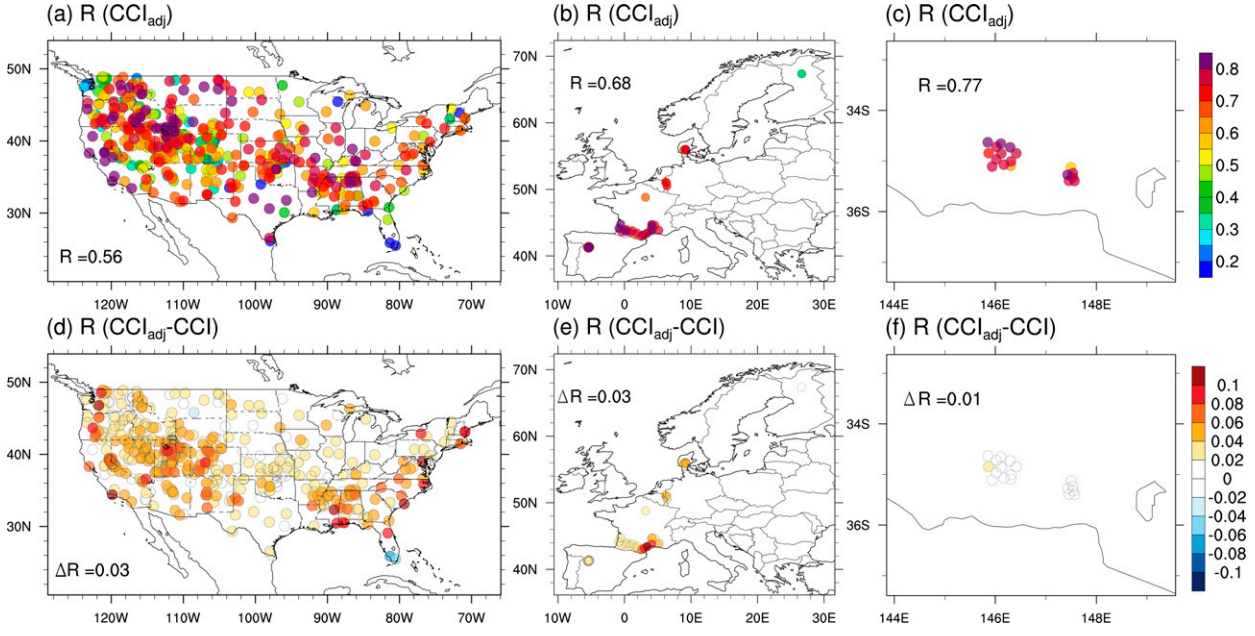

FIG. 7. Surface SM skill measured as the temporal correlation coefficient R between daily in situ measurements and CCI_{adj} over (a) CONUS, (b) Europe, and (c) Australia. (d)–(f) The skill difference between CCI_{adj} and CCI, with red (blue) colors indicating that CCI_{adj} has higher (lower) skill than CCI. Domain averaged R and its difference (CCI_{adj} minus CCI) are indicated near the corner of each map.

The skill of surface SM is measured by the correlation coefficient of SM products against in situ measurements in the continental United States, Europe, and Australia. The average R values of the CCI_{adj} are 0.56, 0.68, and 0.77 in each continent (Figs. 7a–c). The skill of CCI_{adj} is better than that of CCI (ΔR ~0.03, 0.03, and 0.01 over United States, Europe, and Australia, respectively) at nearly every station. Although the skill improvement by the application of the proposed time filtering methodology is greater for CCI version 5.2 (supplemental Fig. 1), which shows lower skill in the unfiltered dataset, there is clear improvement in CCI version 6.1 as well. The skill increase is mostly attributed to the improvement in high-frequency variability, so that the skill measured by the anomaly correlation coefficient, which assesses the daily time series with the 30-day running mean removed, indicates higher correlation for CCI_{adj} by an average of +0.05 (supplemental Fig. 2).

For the comparison of the skill of surface SM between CCI and CCI_{adj} across land cover classes and continent domains, the skill is averaged by these categorizations (Fig. 8). The median correlation skill of surface SM (Fig. 8a) increases for CCI_{adj} by 0.05, compared to CCI (R = 0.57) when averaged over all in situ observation sites. The result implies that the CCI SM time correction provides statistically significant surface SM improvements at a 95% confidence level. The skill improvement is more statistically significant for savannas and grassland than for the other land cover classes, in which the skill of the original CCI surface SM is relatively poor and the number of observations employed in the validation are less. We also demonstrate the skill improvement in the CCI_{adj} compared to CCI categorized by each continental domain (Fig. 8b). Although skill improvement is shown across all locations, the result is statistically significant only over CONUS, likely due to the larger number of observation sites.

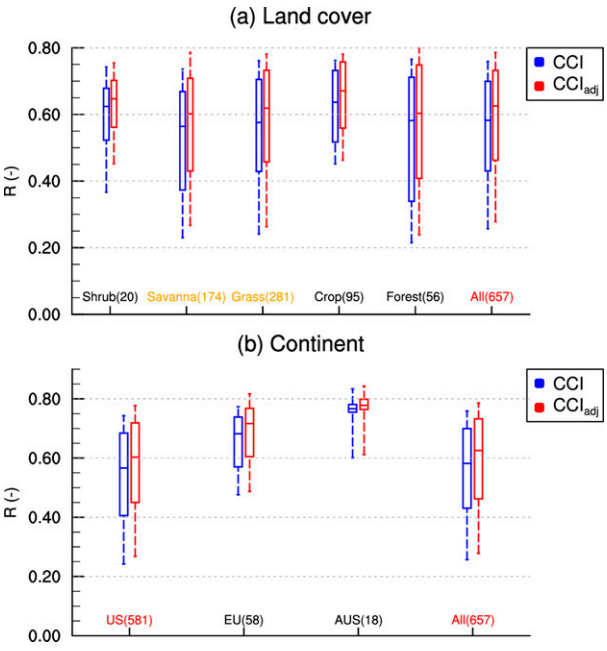

FIG. 8. Boxplot of the correlation coefficient (R) of surface SM from the CCI (blue) and the CCI_{adj} (red) categorized by (a) land cover class and (b) continent. The SM datasets are validated against in situ measurements over CONUS, Europe, and Australia (see Fig. 1 for locations) and categorized by land cover class. Boxes show the median and interquartile range, and whiskers represent the 10th and 90th percentiles. The number of sites used in the validation for each region is shown in parentheses. Orange and red labels in the x axis indicate statistical significance at the 90% and 95% confidence level from the Student's t test, respectively.

b. Improvement of surface SM features

This study adopts the surface SMM, and SME defined in section 3c to explore the SM features in the original CCI and time-filtered CCI_{adj} SM products. For a fair comparison, if any day's data are missing in one time series, the other datasets are masked out for the same day. The surface SMM of the observations is relatively high in the western United States north of ~37°N and in the southeastern United States (Fig. 9a), which is quite similar to the total SM SD (cf. Fig. 4a). The surface SMM map for CCI_{adj} resembles the observed spatial distribution of the SMM (Fig. 9g), more than CCI does (Fig. 9d). The average SMM values of in situ measurements, the CCI, and the CCI_{adj} datasets over the continental United States are 25.3, 10.1, and 17.6 days, respectively, where the SMM from CCI_{adj} over the sites in the best match the observations but tends to overestimate SMM in the western United States. The average SMM values in the European region are 31.4, 22.6, and 33.7 days. For the OZNET network in Australia, the averaged SMM values are 15.7, 15.0, and 20.6 days. When the Fourier-based time filtering is applied to the CCI SM, the surface SMM generally increases as SM autocorrelation increases by removing random noise in the satellite-based SM retrieval. The result is an obvious improvement, although there remains a noticeable underestimation of SMM in CCI_{adj} over CONUS.

The surface SME of the station observations due to random instrument error on the daily time scale is minimal across the domains, at the level of ~0.01 in terms of volumetric soil moisture (Figs. 10a–c), so we have not attempted to adjust these data. However, the averaged surface SME values from the CCI over CONUS, Europe, and Australia are 0.28, 0.23, and 0.08, respectively. The spatial distribution of the CCI SME in CONUS is characterized by stations with high error over the western (west of 105°W) and eastern United States (viz., in forested regions) (Fig. 10d). The large errors in the satellite SM product over the United States are greatly decreased in the CCI_{adj} where the averaged estimated SME from the CCI_{adj} is only 0.04. The averaged values over Europe and Australia are 0.03 and 0.01, respectively, which is comparable level to the observations.

The surface SMM and SME from the in situ observations, the CCI, and the CCI_{adj} are also categorized by land cover classes (Fig. 11). CCI_{adj} commonly represents better agreement with observations across all land cover classes, where the median value of the surface SMM from the observation is 25 days and the values from CCI and CCI_{adj} are 11 and 19 days, respectively (Fig. 11a). The surface SMM improvement

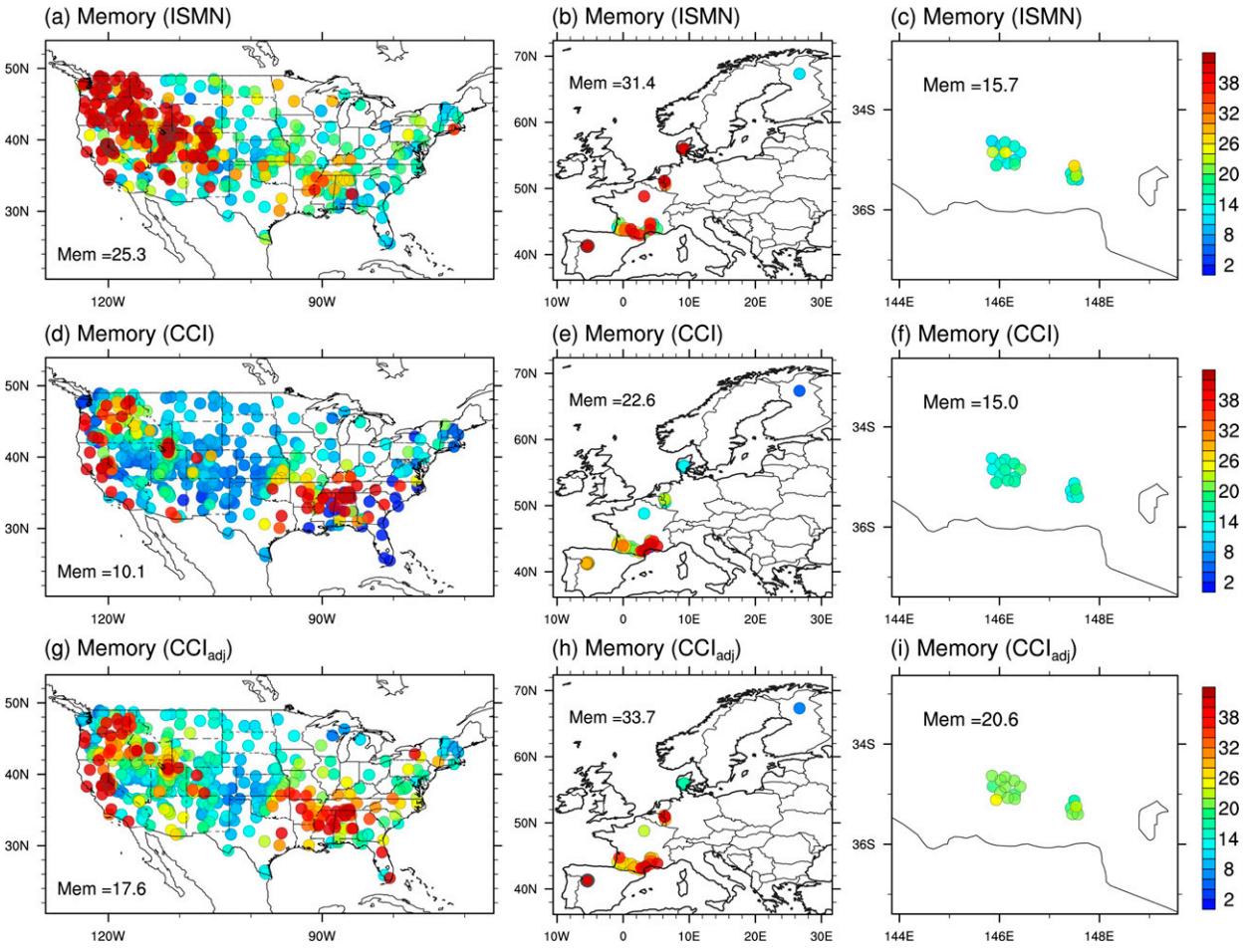

FIG. 9. Surface SM memory (days) from (a)–(c) the in situ measurements, (d)–(f) CCI, and (g)–(i) CCI_{adj} over (left) CONUS, (center) Europe, and (right) Australia. Domain median values of SM memory are indicated near the corner on each map.

is statistically significant at a 95% confidence level for all land cover classes except shrubland. We also show the surface SME categorized by the land cover classes (Fig. 11b). The surface SME of the CCI is the greatest in savannas and forests, and the decrease in SME for CCI_{adj} is statistically significant at the 95% confidence level for all land cover classes. Although the surface SME of CCI v06.1 has been reduced compared to CCI v05.2 (supplemental Fig. 3), likely by the application of gap filling of signal-to-noise ratio depending on land cover types and break-adjusted by using ERA5 reanalysis (Preimesberger et al. 2021), there is still room to reduce the random error component.

For the global distribution change of the surface SMM and SME, Fig. 12 shows the spatial distributions and difference maps for CCI and CCI_{adj}. The spatial patterns of the SMM from CCI and CCI_{adj} are similar (Figs. 12a,b); the spatial correlation between them is 0.62, highest in tropical margins, but the value of the SMM increases in CCI_{adj}. The change of SMM is largest in the Sahara, Arabia, India, South Asia, and CONUS (Fig. 12c). Regions with increased SMM in the United States are spatially consistent with those having high SMM in the observations (cf. Fig. 9a). The SMM and SME have opposite spatial distributions (Fig. 12d); the spatial correlation between them is −0.28. This is related to a decrease in the SM autocorrelation value when the error increases due to the random noise in satellite data, but this component of error is greatly diminished in CCI_{adj} (Fig. 12e) and the error decrease is especially prominent in the Sahara and southeastern United States (Fig. 12f).

Additionally, Fig. 13 compares the surface SMM and SME from CCI and CCI_{adj} products across various land cover classes over the global domain (cf. Fig. 11). The CCI SM data show high SMM in grasslands and croplands, and low in shrublands, savannas, and forest regimes. The change in SMM is statistically significant over the globe and the global median values of the SMM from CCI and CCI_{adj} products are 8 and 12 days, respectively. The relative distributions of the CCI_{adj} SMM according to the land cover class is similar to that of the CCI. The SME in CCI categorized by land cover class is also similar to the observational site analysis (cf. Fig. 11b). The SME is high in shrublands,

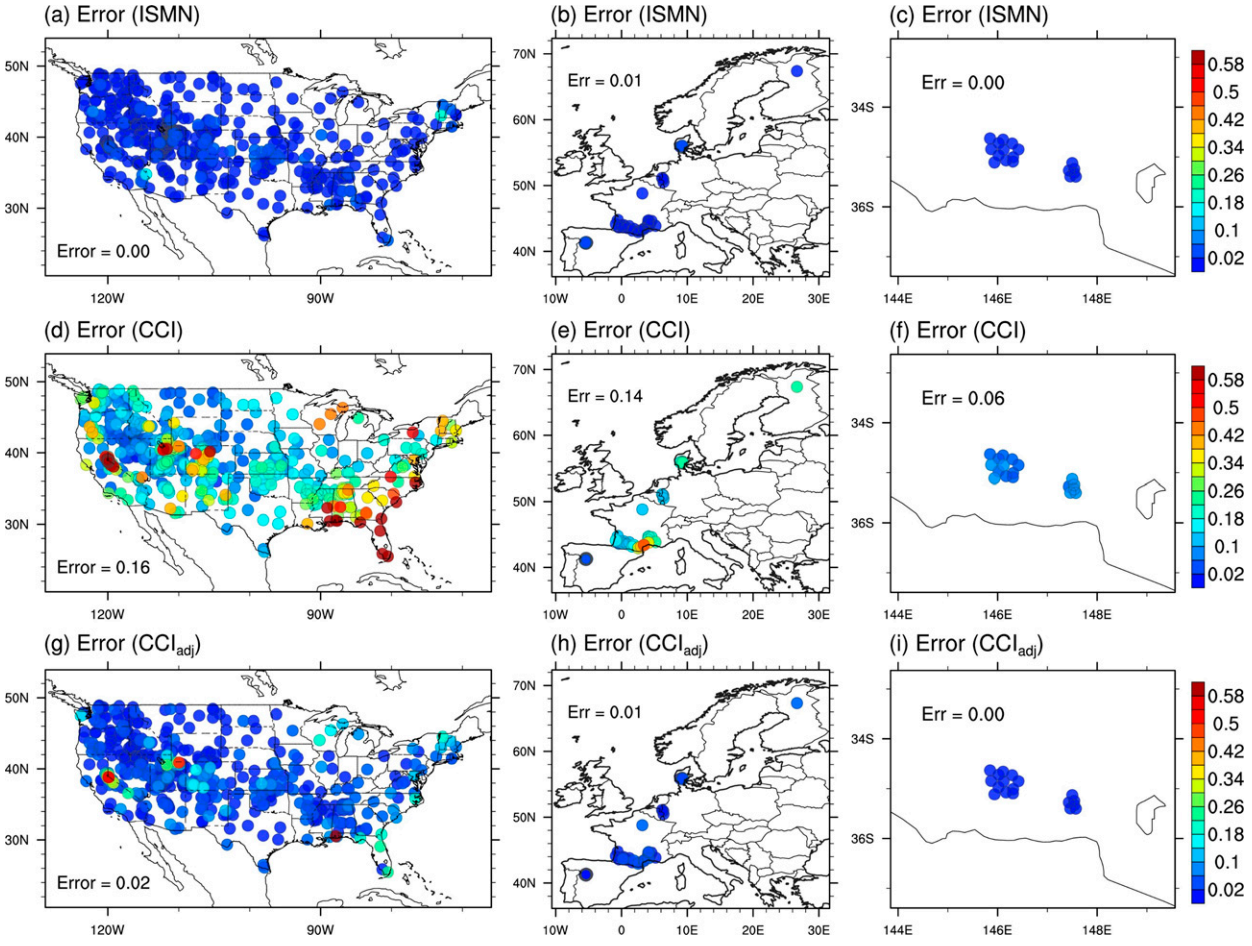

FIG. 10. As in Fig. 9, but for surface SM error.

savannas, barren and forests regions, and low in grasslands and croplands, which is also in opposition to the results for SMM. The decreased SME in the CCI_{adj} is statistically significant over the globe.

5. Conclusions

Only satellite-based SM products can provide global observational estimates to validate and calibrate global models, but only if their SM time series are physically plausible. The ESA CCI SM data unify various single-sensor active and passive microwave SM satellites and provide a global satellite-based observational SM dataset with multidecadal time coverage. Although the CCI SM algorithm harmonizes and merges multiple active and passive satellite SM retrievals to produce a consistently intercalibrated and quality-controlled SM dataset, it does not fully consider the physics of SM dynamics, such that nonphysical noise (random errors) may account for a large portion of the total variability in SM time series, especially at higher frequencies. This greatly affects the usefulness of CCI and other satellite SM products for model validation and application in observationally based estimates of land–atmosphere coupling indices, which quantify interactive surface processes on daily to subseasonal time scales (Santanello et al. 2018).

To address this problem in satellite-retrieved SM products, this study demonstrates the utility of a Fourier-based time filtering method calibrated to physics-based LSM datasets (that include water and energy balance processes) to reduce stochastic random and systematic periodic errors present in the daily CCI SM product. Filtering is conducted across the entire time domain but has the greatest impact on short time scale variations. This study examines the impact of the application of the time filtering method to the CCI SM using several measures of SM skill through validation with ground-based measurements, and its impact on spatial features.

The results reveal that the Fourier-based time filtering method provides added value by better representing surface SM time series over the conterminous United States, Europe, and Australia where in situ surface soil moisture measurements are plentiful. Although the high-frequency CCI SM variability is overestimated by more than 35% compared to observations over CONUS, this large bias is corrected in the Fourier-adjusted CCI_{adj}. Furthermore, the skill improvement in the CCI_{adj} SM measured by temporal correlation of daily values with observations is statistically significant by

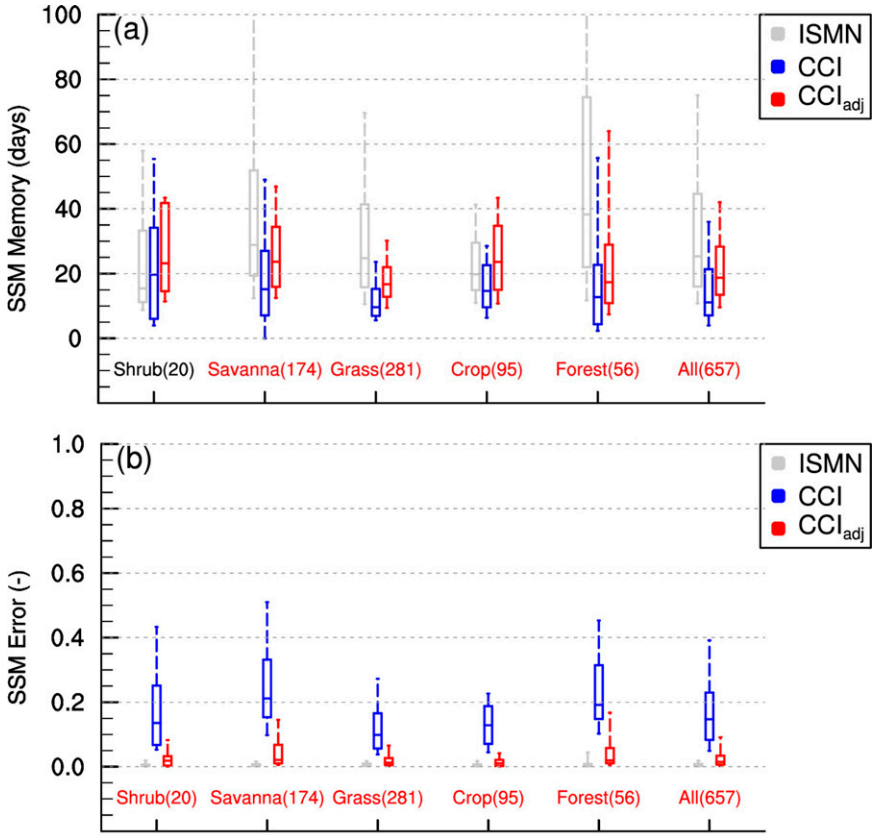

FIG. 11. Boxplot of surface (a) SM memory and (b) SM error from in situ observations (gray), the CCI (blue) and the CCI_{adj} (red) over CONUS, Europe, and Australia categorized by MODIS land cover class. Boxes show the median and interquartile range, and whiskers represent the 10th and 90th percentiles. The number of sites in each category used in the validation is shown in parentheses. A red label indicates statistical significance at the 95% confidence level from the Student's *t* test.

$\Delta R \sim +0.05$, compared to the CCI SM product, appearing more pronounced in savannas and grassland regimes. Also, the skill improvement in the application of the time filtering based on the MME is greater than using any of the individual model products (not shown).

Meanwhile, surface SM memory is generally increased by ameliorating the effect of random measurement noise in the satellite-based SM retrievals. CCI_{adj} represents better agreement with observations in all land cover classes across the observational sites. The surface SMM improvement is statistically significant for most land cover regimes except for shrubland. The median value of the surface SMM from the observations is 25 days and the short-term memory bias in CCI is cut in half by the Fourier adjustment procedure. As the time filtering method removes noise in the CCI SM retrieval, the estimated random SME of the CCI_{adj} is reduced to approximately that of the in situ observations. In the global domain analysis, we confirm that the increased memory and decreased random error in CCI_{adj} are statistically significant over the globe, and especially strong over savannas, barren and forests regions. The increase in the CCI_{adj} SMM extends the global median from 8 to 12 days with a significant decrease in SME.

The time filtering approach proposed in this study only adjusts the power spectrum of CCI toward that of a multimodel ensemble, but the pattern of day-to-day, week-to-week, etc., variability that is crucial to estimating many land–atmosphere coupling metrics still comes from the global satellite product. This approach mainly conducts denoising of the CCI product by effectively damping high-frequency variability, which also leads to increased autocorrelation of SM. Therefore, when the time filtered CCI SM is used to estimate land–atmosphere coupling metrics, coupling strengths are generally increased due to higher magnitudes of correlations (due to reduced random measurement noise) between SM and other variables such as surface heat fluxes, near surface temperature and humidity. Improved SM time series from the time filtering method described in this study can be useful to improve our understanding of the water, energy, and carbon cycles at the land surface, and are a step toward production of global observationally based estimates of land–atmosphere coupling indices.

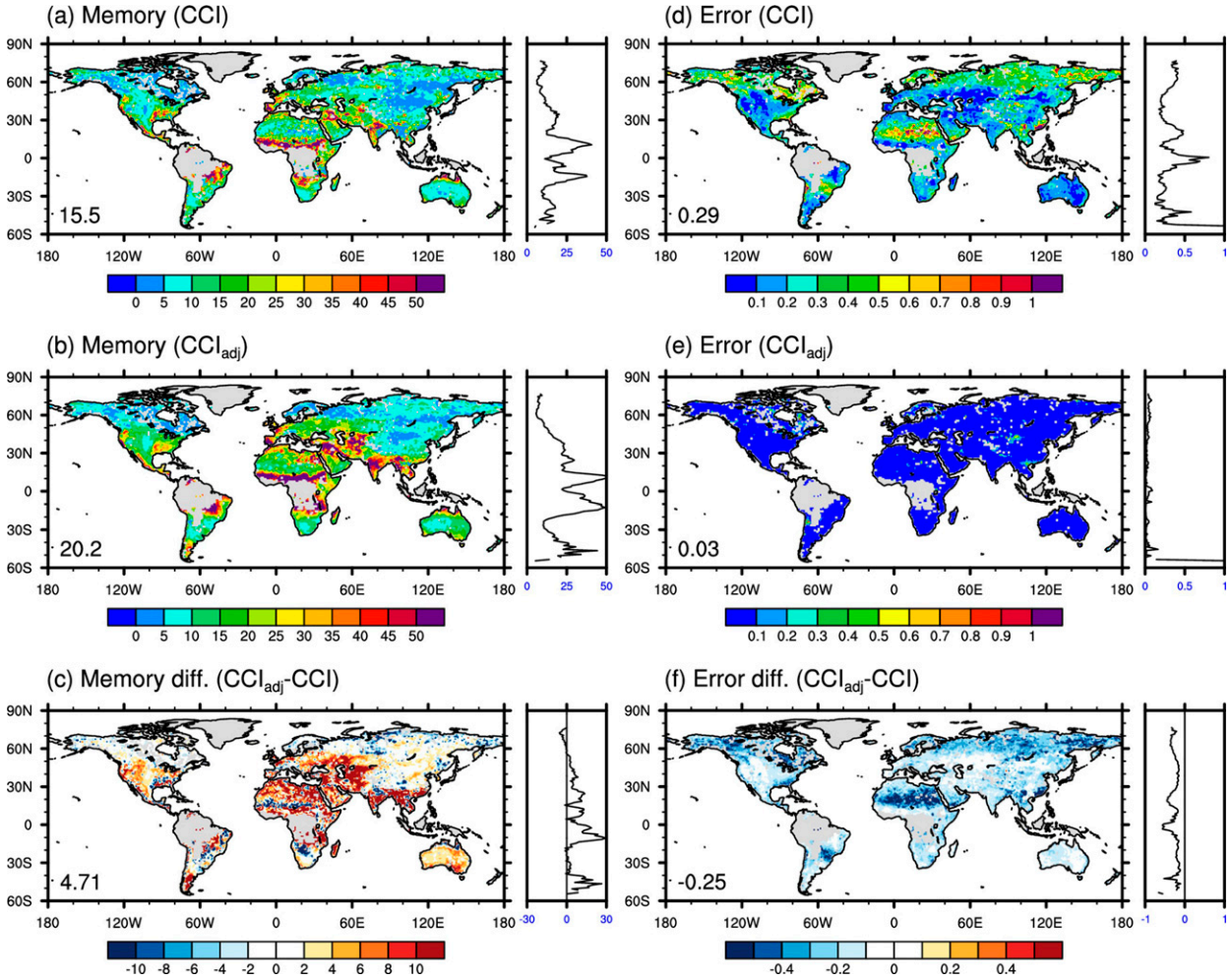

FIG. 12. (a)–(c) Surface SM memory and (d)–(f) SM error from (top) CCI, (middle) CCI_{adj}, and (bottom) the difference between them. The zonal mean profiles are shown to the right of each panel. Global-mean values are indicated in the bottom-left corner of each map.

Furthermore, when land data assimilation combines soil moisture information from diverse satellite observations within the platform of a LSM, e.g., in the context of historical reanalysis, this method could potentially lead to better results from the data assimilation system (Draper et al. 2012; Jasinski et al. 2019; Kumar et al. 2019; Reichle et al. 2021; Seo et al. 2021). However, as this method uses information from long time series of multiple datasets, it is likely not applicable for real-time SM correction (e.g., providing initial states for forecast models) without substantial augmentation. Then again, in forecast applications, systematic SM biases are more of a problem than random errors. The methodology described here aims to improve the utility of satellite SM data for estimating subseasonal time variations in soil moisture commonly used to estimate land–atmosphere coupling metrics, such as SMM, and can provide a more accurate dataset for model validation on global scales.

Acknowledgments. This study was supported by NOAA Grant NA19NES4320002 to the Cooperative Institute for Satellite Earth System Studies (CISESS) at the University of Maryland/ESSIC via a subaward (79785-Z755420) to the Center for Ocean-Land-Atmosphere Studies at George Mason University, and NASA Grant 80NSSC20K1803.

Data availability statement. All datasets used in this study are publicly available: ESA CCI SM are at https://www.esa-soilmoisture-cci.org/; GLDAS-2.1 and MERRA2 SM are at https://disc.gsfc.nasa.gov/; ERA5-Land SM area at https://cds.climate.copernicus.eu/cdsapp#!/dataset/reanalysis-era5-land; and ISMN SM are at https://ismn.geo.tuwien.ac.at/en/. MODIS land surface types are provided by the Integrated Climate Data Center (ICDC) at https://icdc.cen.uni-hamburg.de/en/modis-landsurfacetype.html.

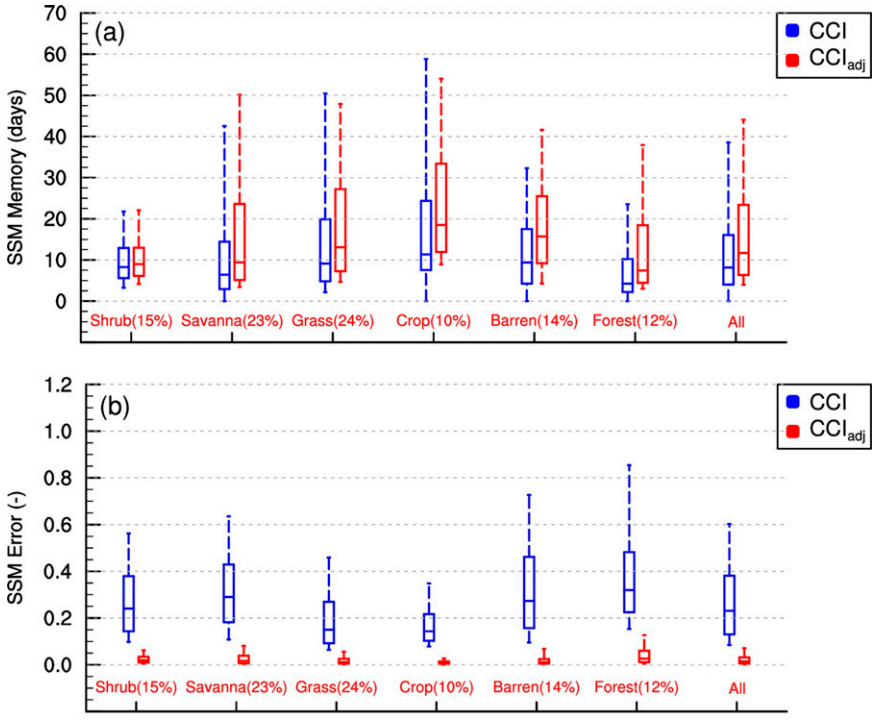

FIG. 13. Boxplot of surface (a) SM memory and (b) SM error from the CCI (blue) and the CCI_{adj} (red) over the globe categorized by MODIS land cover class. Boxes show the median and interquartile range, and whiskers represent the 10th and 90th percentiles. The percent numbers in parentheses along the *x* axis indicate the land coverage frequency relative to the entire global domain. Red labels indicate statistical significance: all are above the 95% confidence level from the Student's *t* test.

REFERENCES

Albergel, C., and Coauthors, 2008: From near-surface to root-zone soil moisture using an exponential filter: An assessment of the method based on in-situ observations and model simulations. *Hydrol. Earth Syst. Sci.*, **12**, 1323–1337, https://doi.org/10.5194/hess-12-1323-2008.

Al-Yaari, A., S. Dayau, C. Chipeaux, C. Aluome, A. Kruszewski, D. Loustau, and J.-P. Wigneron, 2018: The AQUI soil moisture network for satellite microwave remote sensing validation in south-western France. *Remote Sens.*, **10**, 1839, https://doi.org/10.3390/rs10111839.

Bell, J. E., and Coauthors, 2013: U.S. Climate Reference Network soil moisture and temperature observations. *J. Hydrometeor.*, **14**, 977–988, https://doi.org/10.1175/JHM-D-12-0146.1.

Bircher, S., N. Skou, K. Jensen, J. P. Walker, and L. Rasmussen, 2012: A soil moisture and temperature network for SMOS validation in western Denmark. *Hydrol. Earth Syst. Sci.*, **16**, 1445–1463, https://doi.org/10.5194/hess-16-1445-2012.

Calvet, J.-C., N. Fritz, F. Froissard, D. Suquia, A. Petitpa, and B. Piguet, 2007: In situ soil moisture observations for the CAL/VAL of SMOS: The SMOSMANIA network. *2007 IEEE Int. Geoscience and Remote Sensing Symp.*, Denver, CO, Institute of Electrical and Electronics Engineers, 1196–1199, https://doi.org/10.1109/IGARSS.2007.4423019.

Diamond, H. J., and Coauthors, 2013: U.S. Climate Reference Network after one decade of operations: Status and assessment. *Bull. Amer. Meteor. Soc.*, **94**, 485–498, https://doi.org/10.1175/BAMS-D-12-00170.1.

Dirmeyer, P. A., and Coauthors, 2016: Confronting weather and climate models with observational data from soil moisture networks over the United States. *J. Hydrometeor.*, **17**, 1049–1067, https://doi.org/10.1175/JHM-D-15-0196.1.

——, S. Halder, and R. Bombardi, 2018: On the harvest of predictability from land states in a global forecast model. *J. Geophys. Res. Atmos.*, **123**, 13 111–13 127, https://doi.org/10.1029/2018JD029103.

——, G. Balsamo, E. M. Blyth, R. Morrison, and H. M. Cooper, 2021: Land-atmosphere interactions exacerbated the drought and heatwave over northern Europe during summer 2018. *AGU Adv.*, **2**, e2020AV000283, https://doi.org/10.1029/2020AV000283.

Dorigo, W., K. Scipal, R. M. Parinussa, Y. Y. Liu, W. Wagner, R. A. De Jeu, and V. Naeimi, 2010: Error characterisation of global active and passive microwave soil moisture datasets. *Hydrol. Earth Syst. Sci.*, **14**, 2605–2616, https://doi.org/10.5194/hess-14-2605-2010.

——, and Coauthors, 2011: The International Soil Moisture Network: A data hosting facility for global in situ soil moisture measurements. *Hydrol. Earth Syst. Sci.*, **15**, 1675–1698, https://doi.org/10.5194/hess-15-1675-2011.

——, and Coauthors, 2015: Evaluation of the ESA CCI soil moisture product using ground-based observations. *Remote Sens. Environ.*, **162**, 380–395, https://doi.org/10.1016/j.rse.2014.07.023.

——, and Coauthors, 2017: ESA CCI soil moisture for improved Earth system understanding: State-of-the art and future directions. *Remote Sens. Environ.*, **203**, 185–215, https://doi.org/10.1016/j.rse.2017.07.001.

Draper, C., R. Reichle, G. De Lannoy, and Q. Liu, 2012: Assimilation of passive and active microwave soil moisture retrievals. *Geophys. Res. Lett.*, **39**, L04401, https://doi.org/10.1029/2011GL050655.

——, ——, R. de Jeu, V. Naeimi, R. Parinussa, and W. Wagner, 2013: Estimating root mean square errors in remotely sensed soil moisture over continental scale domains. *Remote Sens. Environ.*, **137**, 288–298, https://doi.org/10.1016/j.rse.2013.06.013.

Friedl, M. A., D. Sulla-Menashe, B. Tan, A. Schneider, N. Ramankutty, A. Sibley, and X. Huang, 2010: MODIS collection 5 global land cover: Algorithm refinements and characterization of new datasets. *Remote Sens. Environ.*, **114**, 168–182, https://doi.org/10.1016/j.rse.2009.08.016.

Gelaro, R., and Coauthors, 2017: The Modern-Era Retrospective Analysis for Research and Applications, version 2 (MERRA-2). *J. Climate*, **30**, 5419–5454, https://doi.org/10.1175/JCLI-D-16-0758.1.

González-Zamora, Á., N. Sánchez, M. Pablos, and J. Martínez-Fernández, 2019: CCI soil moisture assessment with SMOS soil moisture and in situ data under different environmental conditions and spatial scales in Spain. *Remote Sens. Environ.*, **225**, 469–482, https://doi.org/10.1016/j.rse.2018.02.010.

Gruber, A., C.-H. Su, S. Zwieback, W. Crow, W. Dorigo, and W. Wagner, 2016: Recent advances in (soil moisture) triple collocation analysis. *Int. J. Appl. Earth Obs. Geoinf.*, **45**, 200–211, https://doi.org/10.1016/j.jag.2015.09.002.

——, W. A. Dorigo, W. Crow, and W. Wagner, 2017: Triple collocation-based merging of satellite soil moisture retrievals. *IEEE Trans. Geosci. Remote Sens.*, **55**, 6780–6792, https://doi.org/10.1109/TGRS.2017.2734070.

——, T. Scanlon, R. Schalie, W. Wagner, and W. Dorigo, 2019: Evolution of the ESA CCI soil moisture climate data records and their underlying merging methodology. *Earth Syst. Sci. Data*, **11**, 717–739, https://doi.org/10.5194/essd-11-717-2019.

——, and Coauthors, 2020: Validation practices for satellite soil moisture retrievals: What are (the) errors? *Remote Sens. Environ.*, **244**, 111806, https://doi.org/10.1016/j.rse.2020.111806.

Guo, Z., and P. A. Dirmeyer, 2006: Evaluation of the Second Global Soil Wetness Project soil moisture simulations: 1. Intermodel comparison. *J. Geophys. Res.*, **111**, D22S02, https://doi.org/10.1029/2006JD007233.

——, ——, Z.-Z. Hu, X. Gao, and M. Zhao, 2006: Evaluation of the Second Global Soil Wetness Project soil moisture simulations: 2. Sensitivity to external meteorological forcing. *J. Geophys. Res.*, **111**, D22S03, https://doi.org/10.1029/2006JD007845.

——, ——, X. Gao, and M. Zhao, 2007: Improving the quality of simulated soil moisture with a multi-model ensemble approach. *Quart. J. Roy. Meteor. Soc.*, **133**, 731–747, https://doi.org/10.1002/qj.48.

Huffman, G. J., and Coauthors, 2001: Global precipitation at one-degree daily resolution from multisatellite observations. *J. Hydrometeor.*, **2**, 36–50, https://doi.org/10.1175/1525-7541(2001)002<0036:GPAODD>2.0.CO;2.

Jackson, T. J., and Coauthors, 2010: Validation of advanced microwave scanning radiometer soil moisture products. *IEEE Trans. Geosci. Remote Sens.*, **48**, 4256–4272, https://doi.org/10.1109/TGRS.2010.2051035.

Jasinski, M. F., and Coauthors, 2019: NCA-LDAS: Overview and analysis of hydrologic trends for the national climate assessment. *J. Hydrometeor.*, **20**, 1595–1617, https://doi.org/10.1175/JHM-D-17-0234.1.

Jensen, K. H., and J. C. Refsgaard, 2018: HOBE: The Danish hydrological observatory. *Vadose Zone J.*, **17**(1), 1–24, https://doi.org/10.2136/vzj2018.03.0059.

Koster, R. D., M. J. Suarez, A. Ducharne, M. Stieglitz, and P. Kumar, 2000: A catchment-based approach to modeling land surface processes in a general circulation model: 1. Model structure. *J. Geophys. Res.*, **105**, 24 809–24 822, https://doi.org/10.1029/2000JD900327.

——, and Coauthors, 2004: Realistic initialization of land surface states: Impacts on subseasonal forecast skill. *J. Hydrometeor.*, **5**, 1049–1063, https://doi.org/10.1175/JHM-387.1.

Kumar, S. V., and Coauthors, 2019: NCA-LDAS land analysis: Development and performance of a multisensor, multivariate land data assimilation system for the National Climate Assessment. *J. Hydrometeor.*, **20**, 1571–1593, https://doi.org/10.1175/JHM-D-17-0125.1.

Larson, K. M., E. E. Small, E. D. Gutmann, A. L. Bilich, J. J. Braun, and V. U. Zavorotny, 2008: Use of GPS receivers as a soil moisture network for water cycle studies. *Geophys. Res. Lett.*, **35**, L24405, https://doi.org/10.1029/2008GL036013.

Lei, F., W. T. Crow, H. Shen, C.-H. Su, T. R. Holmes, R. M. Parinussa, and G. Wang, 2018: Assessment of the impact of spatial heterogeneity on microwave satellite soil moisture periodic error. *Remote Sens. Environ.*, **205**, 85–99, https://doi.org/10.1016/j.rse.2017.11.002.

Loveland, T. R., and A. Belward, 1997: The IGBP-DIS global 1km land cover data set, DISCover: First results. *Int. J. Remote Sens.*, **18**, 3289–3295, https://doi.org/10.1080/014311697217099.

Massari, C., C.-H. Su, L. Brocca, Y.-F. Sang, L. Ciabatta, D. Ryu, and W. Wagner, 2017: Near real time de-noising of satellite-based soil moisture retrievals: An intercomparison among three different techniques. *Remote Sens. Environ.*, **198**, 17–29, https://doi.org/10.1016/j.rse.2017.05.037.

Preimesberger, W., T. Scanlon, C.-H. Su, A. Gruber, and W. Dorigo, 2021: Homogenization of structural breaks in the global ESA CCI soil moisture multisatellite climate data record. *IEEE Trans. Geosci. Remote Sens.*, **59**, 2845–2862, https://doi.org/10.1109/TGRS.2020.3012896.

Reichle, R. H., R. D. Koster, J. Dong, and A. A. Berg, 2004: Global soil moisture from satellite observations, land surface models, and ground data: Implications for data assimilation. *J. Hydrometeor.*, **5**, 430–442, https://doi.org/10.1175/1525-7541(2004)005<0430:GSMFSO>2.0.CO;2.

——, S. Q. Zhang, Q. Liu, C. S. Draper, J. Kolassa, and R. Todling, 2021: Assimilation of SMAP brightness temperature observations in the GEOS land–atmosphere data assimilation system. *IEEE J. Sel. Top. Appl. Earth Obs. Remote Sens.*, **14**, 10 628–10 643, https://doi.org/10.1109/JSTARS.2021.3118595.

Robock, A., K. Y. Vinnikov, C. A. Schlosser, N. A. Speranskaya, and Y. Xue, 1995: Use of midlatitude soil moisture and meteorological observations to validate soil moisture simulations with biosphere and bucket models. *J. Climate*, **8**, 15–35, https://doi.org/10.1175/1520-0442(1995)008<0015:UOMSMA>2.0.CO;2.

Rodell, M., and Coauthors, 2004: The global land data assimilation system. *Bull. Amer. Meteor. Soc.*, **85**, 381–394, https://doi.org/10.1175/BAMS-85-3-381.

Santanello, J. A., Jr., and Coauthors, 2018: Land–atmosphere interactions: The LoCo perspective. *Bull. Amer. Meteor. Soc.*, **99**, 1253–1272, https://doi.org/10.1175/BAMS-D-17-0001.1.

Schaefer, G. L., M. H. Cosh, and T. J. Jackson, 2007: The USDA natural resources conservation service Soil Climate Analysis

Network (SCAN). *J. Atmos. Oceanic Technol.*, **24**, 2073–2077, https://doi.org/10.1175/2007JTECHA930.1.

Seneviratne, S. I., and Coauthors, 2010: Investigating soil moisture–climate interactions in a changing climate: A review. *Earth-Sci. Rev.*, **99**, 125–161, https://doi.org/10.1016/j.earscirev.2010.02.004.

Seo, E., and Coauthors, 2019: Impact of soil moisture initialization on boreal summer subseasonal forecasts: Mid-latitude surface air temperature and heat wave events. *Climate Dyn.*, **52**, 1695–1709, https://doi.org/10.1007/s00382-018-4221-4.

——, M.-I. Lee, S. D. Schubert, R. D. Koster, and H.-S. Kang, 2020: Investigation of the 2016 Eurasia heat wave as an event of the recent warming. *Environ. Res. Lett.*, **15**, 114018, https://doi.org/10.1088/1748-9326/abbbae.

——, ——, and R. H. Reichle, 2021: Assimilation of SMAP and ASCAT soil moisture retrievals into the JULES land surface model using the Local Ensemble Transform Kalman Filter. *Remote Sens. Environ.*, **253**, 112222, https://doi.org/10.1016/j.rse.2020.112222.

Smith, A. B., and Coauthors, 2012: The Murrumbidgee soil moisture monitoring network data set. *Water Resour. Res.*, **48**, W07701, https://doi.org/10.1029/2012WR011976.

Su, C.-H., and D. Ryu, 2015: Multi-scale analysis of bias correction of soil moisture. *Hydrol. Earth Syst. Sci.*, **19**, 17–31, https://doi.org/10.5194/hess-19-17-2015.

——, ——, A. W. Western, and W. Wagner, 2013: De-noising of passive and active microwave satellite soil moisture time series. *Geophys. Res. Lett.*, **40**, 3624–3630, https://doi.org/10.1002/grl.50695.

——, J. Zhang, A. Gruber, R. Parinussa, D. Ryu, W. T. Crow, and W. Wagner, 2016: Error decomposition of nine passive and active microwave satellite soil moisture data sets over Australia. *Remote Sens. Environ.*, **182**, 128–140, https://doi.org/10.1016/j.rse.2016.05.008.

Vinnikov, K. Y., and I. Yeserkepova, 1991: Soil moisture: Empirical data and model results. *J. Climate*, **4**, 66–79, https://doi.org/10.1175/1520-0442(1991)004<0066:SMEDAM>2.0.CO;2.

——, A. Robock, N. A. Speranskaya, and C. A. Schlosser, 1996: Scales of temporal and spatial variability of midlatitude soil moisture. *J. Geophys. Res.*, **101**, 7163–7174, https://doi.org/10.1029/95JD02753.

Zacharias, S., and Coauthors, 2011: A network of terrestrial environmental observatories in Germany. *Vadose Zone J.*, **10**, 955–973, https://doi.org/10.2136/vzj2010.0139.

Zreda, M., W. Shuttleworth, X. Zeng, C. Zweck, D. Desilets, T. Franz, and R. Rosolem, 2012: COSMOS: The cosmic-ray soil moisture observing system. *Hydrol. Earth Syst. Sci.*, **16**, 4079–4099, https://doi.org/10.5194/hess-16-4079-2012.